THE SARDINIA RADIO TELESCOPE: A COMPARISON BETWEEN CLOSE RANGE PHOTOGRAMMETRY AND FE MODELS

FRANCO BUFFA, ANDREA CAUSIN, ANTONIO CAZZANI, SERGIO POPPI, GIANNINA SANNA, MARGHERITA SOLCI, FLAVIO STOCHINO, AND EMILIO TURCO

Dedicated to Dr. R. A. Toupin in recognition of his outstanding contribution to Mechanics

Abstract. The Sardinia Radio Telescope (SRT), located near Cagliari (Italy), is the world's second largest fully steerable radio telescope endowed with an active–surface system. Its primary mirror has a quasi–parabolic shape with a diameter of 64 m. The configuration of the primary mirror surface can be modified by means of electro–mechanical actuators. This capability ensures, within a fixed range, the balancing of the deformation caused, for example, by loads such as self–weight, thermal effects and wind pressure. In this way, the difference between the ideal shape of the mirror (which maximizes its performances) and the actual surface can be reduced. In this paper the authors describe the characteristics of SRT, the Close Range Photogrammetry (CRP) survey developed in order to set up the actuators displacements and a Finite Element model capable of accurately estimating the structural deformations. Numerical results have been compared with CRP measurements in order to test the accuracy of the model.

1. Introduction

Radio telescopes are antennas devoted to the analysis and the study of celestial objects, collecting the radiation emitted in the radio region of the electromagnetic spectrum (see Figure 1). The received signals are extremely weak, thus large collecting areas are required. Moreover, the larger the size of a radio telescope, the better its angular resolution is. Nevertheless, large instruments are more sensible to the deformations of its structure, because of gravity, temperature and wind.

In order to contrast the gravitational effects, radio telescopes may be equipped with the so–called Active surface System (AS), complex devices designed to modify in real time the antenna shape.

Radio telescope deformations can be distinguished in spatially large–scale deformations, affecting the pointing and the focus, and small–scale deformations, which can decrease the efficiency of the telescope.

The efficiency of a radio telescope is described by the aperture efficiency η_A, see [1], defined by:

$$\eta_A = \frac{A}{A_g}\,. \tag{1}$$

Date: April 20, 2021.

Key words and phrases. Sardinia Radio Telescope, Finite Element Models, Structural Modelling, Huge Structures, Active Structures, High precision measurements.

(a) SRT view 1

(b) SRT view 2

FIGURE 1. SRT parts: 1) Reinforced concrete basament and fundation. 2) Alidade. 3) Back Up Structure. 4) Principal Mirror (M1). 5) Thermal Shield (it has not been placed in the real structure although it was expected to be present in the designed one). 6) Quadrupod Structure. 7) Secondary Mirror (M2).

Please cite this document as: F. Buffa, A. Causin, A. Cazzani, S. Poppi, G. Sanna, M. Solci, F. Stochino, and E. Turco "The Sardinia Radio Telescope: A comparison between close-range photogrammetry and finite element models" Mathematics and Mechanics of Solids, 2017, Vol. 22(5): 1005-1026 doi:10.1177/1081286515616227

where A_g is the *geometric* area and A denotes the *effective* area, that is the area effectively contributing to collect the incoming radiation. The aperture efficiency η_A takes into account many different effects; in particular, the effective area A depends on the surface-loss efficiency η_s, which measures the losses due to the small–scale randomly distributed deviations of the reflector from the ideal shape. It is expressed by the Ruze's law [2]:

$$\eta_s = \exp\left(-\left(\frac{4\pi\delta_{RMS}}{\lambda}\right)^2\right), \tag{2}$$

where λ is the radiation wavelength and δ_{RMS} is the global Root Mean Square (RMS) deviation from the ideal reflector shape, defined by:

$$\delta_{RMS} = \left(\frac{1}{|\Omega|}\int_\Omega (\tilde{g} - g)^2 d\Omega\right)^{1/2}, \tag{3}$$

where g is the theoretical shape of the reflector and $\tilde{g}$ the actual one, while $|\Omega|$ is the measure of the surface (reflector) area.

Note that η_s increases when wavelength decreases, so that surface loss efficiency becomes critical for higher frequencies. The dependence of η_s from δ_{RMS} implies that to maximize the efficiency (in the ideal case, to have $\eta_s \approx 1$) a control on δ_{RMS}/λ is required. In particular, for a good efficiency value ($\eta_s = 53\%$), δ_{RMS} should be lower than $\lambda/16$, or at least lower than $\lambda/10$ for the minimum–acceptable efficiency value ($\eta_s = 20\%$).

In order to correct the deformations in real time by means of the AS, during the telescope operations, a measuring technique is needed for evaluating them. Alternatively a sensor network gathering information for their modeling and providing data to the telescope control system has to be installed.

Close range photogrammetry is a non–contact measuring technique widely used in radio astronomical field for the representation of the shape of large antennas. The first applications of this method to radio telescopes were the measurements of the 300–ft (91.44 m) and 85–ft (25.91 m) antennas at the National Radio Astronomy Observatory (NRAO) in Green Bank, West Virginia, in 1962 [3], with a camera hosted on a helicopter, achieving an accuracy of 1 mm over the 100–meter size of the telescope. Afterwards, it has been used in the setting of one of the 12 m diameter Atacama Large Millimeter/submillimeter Array (ALMA) antennas [1], with a fully digital system achieving an accuracy of 0.030 mm, that is a part over 1 million.

Recently, photogrammetry methods have been applied also to the Sardinia Radio Telescope antenna. In this paper, we aim to compare photogrammetric data, obtained during the alignment of its primary mirror [4], to the finite element models of the whole structure [5].

In Section 2 a description of SRT is presented; photogrammetric measurements are described in Section 3 while the Finite Element (FE) numerical model and its results are presented respectively in Sections 4 and 5. Finally conclusions and new research perspectives are drawn in Section 6.

2. The Sardinia Radio Telescope

The Sardinia Radio Telescope is a fully steerable antenna for observing the sky at frequency between 300 MHz and 100 GHz. It has a Gregorian configuration, with a quasi parabolic shaped primary mirror (M1) and an elliptical shaped secondary mirror (M2), see again Figure 1. Its highest operating frequency, 100 GHz, corresponds to a wavelength of 3 mm. Thus, according to Ruze's law, the good efficiency value requires that the geometric

Please cite this document as: F. Buffa, A. Causin, A. Cazzani, S. Poppi, G. Sanna, M. Solci, F. Stochino, and E. Turco "The Sardinia Radio Telescope: A comparison between close-range photogrammetry and finite element models" Mathematics and Mechanics of Solids, 2017, Vol. 22(5): 1005-1026 doi:10.1177/1081286515616227

deformations from its ideal shape must be kept below 0.185 mm for δ_{RMS}, or 0.3 mm if the minimum–acceptable value is taken into account. To this end, SRT is provided with an active surface system [6]. The primary mirror consists of 1008 aluminum panels, and 1116 actuators with a stroke of 30 mm mounted on the backup structure. Each actuator is supported by studs and can move at the same time the corners of the four (or the two) nearest panels, in the direction normal to the local surface. They are organized in 96 radial lines with a minimum of 9 and maximum of 16 actuators for each line. Actuators work in a way that they can remove the small–scale deformations, while large scale deformations are reduced by a correction in pointing and by secondary mirror movements.

During the construction phase, thanks to photogrammetry, panels were aligned by hand reaching a global RMS of about 0.3 mm for the 45° telescope elevation. However with the actuators up and running this alignment precision may be reached over the whole elevation range, provided that panels deformation could be measured/estimated with the same or with a better precision.

FIGURE 2. Setting for a photogrammetric measurements at SRT.

3. PHOTOGRAMMETRIC MEASUREMENTS

As stated before, Close Range Photogrammetry (CRP) has been widely used throughout the whole process of SRT construction. The reason of this choice lies in its good combination of precision and survey speediness, so that CRP has been preferred with respect to other survey techniques such as topographic survey with Total Station or laser tracker [4].

Indeed, CRP can reach a very high precision if few precautions are taken. Among them:

- multi–image acquisition, taken all around the object in order to simultaneously enable camera calibration by means of a bundle adjustment procedure (in any case the use of metric cameras is mandatory), over–determination of each point of measure for outlier detection, equally distribute sigmas for the three point coordinates;
- specific signalization of measurement points with artificial targets providing unambiguous definition and automatic point identification;
- stability of environmental conditions.

Please cite this document as: F. Buffa, A. Causin, A. Cazzani, S. Poppi, G. Sanna, M. Solci, F. Stochino, and E. Turco "The Sardinia Radio Telescope: A comparison between close-range photogrammetry and finite element models" Mathematics and Mechanics of Solids, 2017, Vol. 22(5): 1005-1026 doi:10.1177/1081286515616227

Denoting by Σ_x the precision in the object with respect to the variable x, the precision in the space coordinate determination can be estimated by:

$$\Sigma_x = qm\sigma_x \,, \tag{4}$$

where m the image scale factor, σ_x the precision in the image space and q a design factor depending on the geometry of the configuration, on datum orientation accuracy, on deformation factor (spatial configuration of bundles) and on control elements factor (accuracy of reference points). It may be the same with respect to the three spatial variables x, y and z or it may be higher along the viewing direction if the object cannot be shot from all sides.

Values of q may vary between 0.4–0.8 for very good configurations and up to 2–3 in weak conditions [7]. Considering an average q value of 0.6 for a good configuration, as it must be in metrological applications, and an average σ_x value of 0.08 μm, Σ_x may vary between 0.024 mm and 0.096 mm if the scale factor m varies between 500 up to 2000. These values have been actually accomplished in SRT case.

Photogrammetric measurements have been performed by the *Sigma3d Company* taking into account the different antenna parts:

(1) subreflector panel alignment in which a tolerance of 0.05 mm (global RMS) was specified;
(2) Back Up Structure (BUS) deflection verification in which the structure deformation between elevation 90° and 37° had to be inside the 20% to that estimated by the FE model;
(3) main reflector panel alignment at 45° in which a tolerance of 0.5 mm (global RMS) was specified;
(4) main reflector adjacent panels corner alignment in which a tolerance of ±0.1 mm was specified;
(5) main reflector deflections at the six elevation positions 90°, 75°, 60°, 45°, 30° and 15°.

Between the above mentioned tasks only the last one is of interest for this paper. For each of the six elevations considered, a set of measurements covering the entire mirror was performed, in order to determine shape deviations from the ideal surface in a panel–wise way. The whole survey has been performed during one night in order to fulfill the environmental specifications regarding wind speed, dew point and temperature variation.

The six measurement sets were compared with the ideal surface taking into account only the small scale displacements. To do so, a best fitting coordinate transformation from the real to the ideal coordinates was estimated, leaving as many degrees of freedom as many real movements the telescope may do to compensate for. The outcome of this last photogrammetric task was a look up table containing the displacements of all the actuators, in each of the six elevation positions, computed in the normal direction to the local surface, to use them directly as movements to give in order to reach a global δ_{RMS} = 0.3 mm or better. Some of these look up tables are presented in a graphic form in Figures 3 (15° elevation), 4 (60° elevation), 5 (75° elevation), 6 (90° elevation).

4. Description of FE models of SRT

A powerful and widespread method for describing the mechanical response of a structure is the FE method [8]. It allows simulating the structural performance for a wide range of configurations/load conditions. During the design stage of SRT several Finite Element

Please cite this document as: F. Buffa, A. Causin, A. Cazzani, S. Poppi, G. Sanna, M. Solci, F. Stochino, and E. Turco "The Sardinia Radio Telescope: A comparison between close-range photogrammetry and finite element models" Mathematics and Mechanics of Solids, 2017, Vol. 22(5): 1005-1026 doi:10.1177/1081286515616227

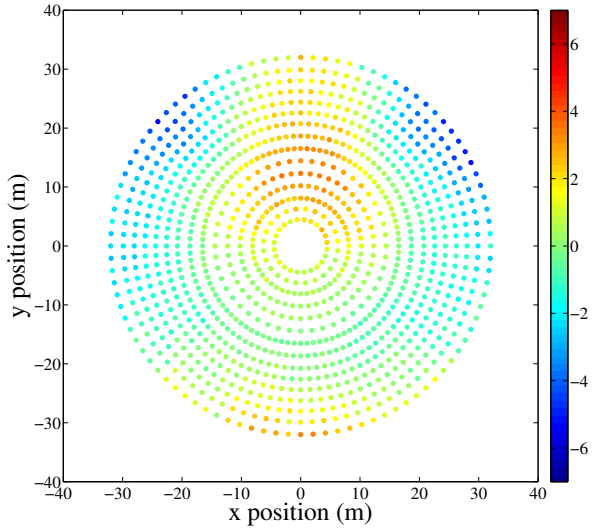

FIGURE 3. Graphical rendering of CRP–deduced look up table for displacement of each actuator at 15° elevation (chromatic scale is in mm).

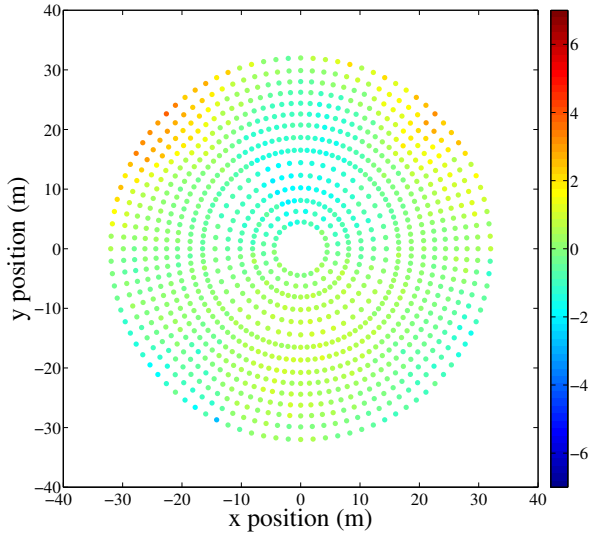

FIGURE 4. Graphical rendering of CRP–deduced look up table for displacement of each actuator at 60° elevation (chromatic scale is in mm).

models were prepared. In particular an ANSYS FE model (see [9]) was built by *BCV Progetti*. The last version of it (v.37), still including the thermal shield, which was originally designed to wrap the rear part of the backup structure is described here, see Figure 7.

Please cite this document as: F. Buffa, A. Causin, A. Cazzani, S. Poppi, G. Sanna, M. Solci, F. Stochino, and E. Turco "The Sardinia Radio Telescope: A comparison between close-range photogrammetry and finite element models" Mathematics and Mechanics of Solids, 2017, Vol. 22(5): 1005-1026 doi:10.1177/1081286515616227

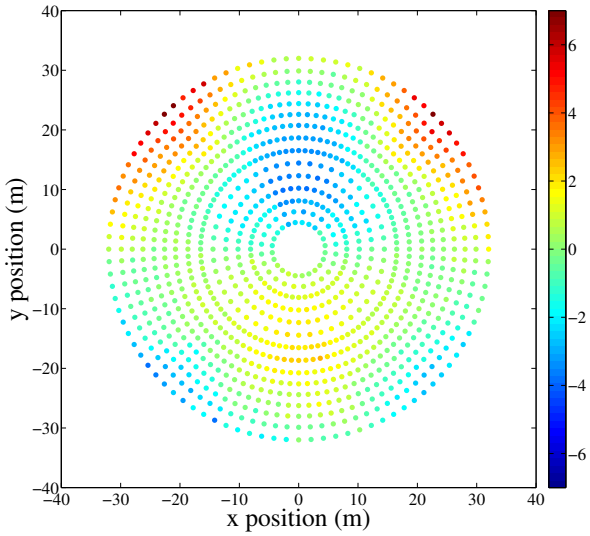

FIGURE 5. Graphical rendering of CRP–deduced look up table for displacement of each actuator at 75° elevation (chromatic scale is in mm).

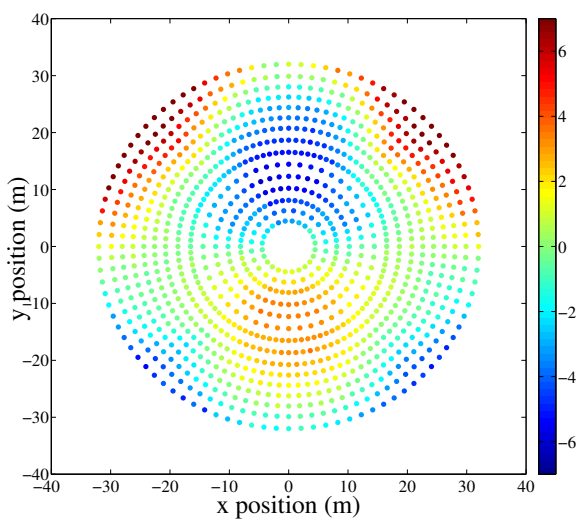

FIGURE 6. Graphical rendering of CRP–deduced look up table for displacement of each actuator at 90° elevation (chromatic scale is in mm).

It consists of 92788 nodes, 94140 elements and a total amount of 463871 degrees–of–freedom. Even with such a complexity the computational cost of a linear elastic static run is quite limited and a popular personal computer can obtain the results in less than one minute.

Please cite this document as: F. Buffa, A. Causin, A. Cazzani, S. Poppi, G. Sanna, M. Solci, F. Stochino, and E. Turco "The Sardinia Radio Telescope: A comparison between close-range photogrammetry and finite element models" Mathematics and Mechanics of Solids, 2017, Vol. 22(5): 1005-1026 doi:10.1177/1081286515616227

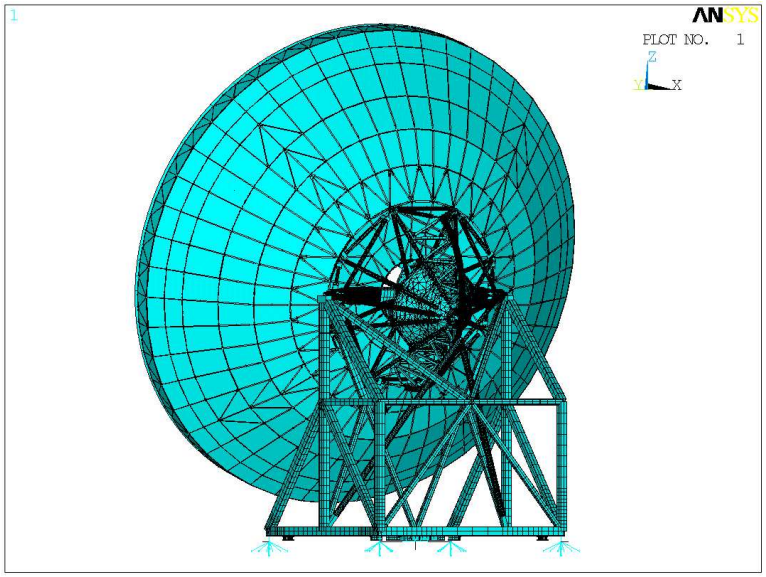

FIGURE 7. Back view of the SRT FE model (including the Thermal Shield) at elevation 15°.

In a bottom–up sequence, the following parts might be singled out (see Figure 1 and Figures 7–8):

(1) *Reinforced concrete basement and foundation rail*: they have been considered as perfectly rigid bodies and have not been modeled. Indeed they have been carefully designed to guarantee the verticality of the azimuth axis. Suitable displacement constraints have been inserted at the end of the base.
(2) *Alidade*: represents the 3–D truss structure which supports the portion of SRT (back up structure, principal mirror, thermal shield, quadrupode, secondary mirror) which can tilt about the elevation axis. It is modeled by means of 2–noded Timoshenko's beam elements with seven degrees–of–freedom per node (taking into account warping, too), and by 2–noded beam elements with six degrees of freedom per node. The latter group allows for independent end–release conditions, which are useful for correctly representing a 3–D truss member.
(3) *Back Up Structure*: it is the structure, shaped like a portion of elliptic paraboloid which supports the antenna of SRT. It is represented by a complex 3–D truss system. Each structural member is modeled by at least four 2–noded beam elements with six degrees of freedom at each node.
(4) *Main reflector (M1)*, *i.e.* principal mirror: it is placed on the front surface of the back up structure and is composed by 1008 panels, each of them is linked to the back up structure by means of a rigid multi–point–constraint element. Any panel is represented by a single shell element with four nodes and six degrees of freedom at each node. Only membrane stiffness is considered.
(5) *Thermal shield*: it is placed on the rear surface of the back up structure and is composed by 505 panels. Each panel, which is directly attached to the nodes of the BUS, is represented by a single shell element with three or four nodes and six degrees of freedom at each node. Only membrane stiffness is considered.

Please cite this document as: F. Buffa, A. Causin, A. Cazzani, S. Poppi, G. Sanna, M. Solci, F. Stochino, and E. Turco "The Sardinia Radio Telescope: A comparison between close-range photogrammetry and finite element models" Mathematics and Mechanics of Solids, 2017, Vol. 22(5): 1005-1026 doi:10.1177/1081286515616227

(6) *Quadrupod structure*: it is made of a four–legged truss structure which supports the secondary mirror. It is modeled by a mixture of two–noded Timoshenko's beam elements and four–noded shell elements with six degrees of freedom per node. In this case shell elements have both bending and membrane stiffness accounted for.

(7) *Secondary mirror (M2)*: only the support structure has been modeled by multi–point–constraint elements and lumped mass elements. Panels have not been explicitly modeled.

From the mechanical point of view, the steel members (alidade, BUS, quadrupod) are represented by an isotropic material model characterized by Young's modulus $E_s = 199.95$ GPa; Poisson's ratio $\nu_s = 0.29464$; density $\rho_s = 7908.5$ kg/m^3; linear thermal expansion coefficient $\alpha_s = 1.17 \times 10^{-5}$ °C^{-1}. The principal mirror reflecting surface is composed of an aluminum alloy whose structural role is negligible and therefore has been represented by a linear isotropic material with a very low value of Young's modulus ($E_a = 0.689$ GPa), Poisson's ratio $\nu_a = 0.29$ and density $\rho_a = 7086.5$ kg/m^3. Similarly, the thermal shield is made of another aluminum alloy with mechanical characteristics equal to the latter but with a different density, equal to $\rho_t = 4961.9$ kg/m^3. The total weight of the model is approximately 32259 kN.

Considering the low–intensity loading experienced by SRT, which for the standard calibration phase is subjected only to gravitational forces and to actuators displacements, the numerical model of the structure was formulated under the assumption of infinitesimal strains and linear elastic behavior of all materials.

However, the thermal shield described in point 5 above, which in the design stage was expected to cover the BUS, providing thermal insulation, was not mounted on SRT, consequently, another FE model of it, taking into account the absence of this part, has been developed by our research group, see Figure 8. For this model the number of elements decreased to 93635 while the total amounts of degrees of freedom and the number of nodes remain the same. The total weight has been reduced to 31730 kN.

5. Analysis of results and comparisons

Photogrammetric measurements (CRP) yield a set of actuators displacements which can be interpreted as a synthetic measure of the deformation of the SRT principal mirror see Figures 3–6. The FE models have been compared with these CRP data. Before proceeding to this comparison it is necessary to transform the FE results (which typically provide x–, y–, z–components of displacements at all nodes) to components of displacements along the unit normal at all points where actuators are placed, *i.e.* at the corners between four panels of the principal mirror.

In order to really understand this problem it is better to depict it from a mathematical point of view: let us assume that $\mathbf{x}_\beta$ is a vector which collects points of the ideal shape of the primary mirror at elevation β, see Figure 9, and $\tilde{\mathbf{x}}_\beta$ the analogous vector collecting the corresponding positions of the same points of the actual shape. Difference $\tilde{\mathbf{x}}_\beta - \mathbf{x}_\beta$ defines the displacement vector $\mathbf{u}_\beta$ which depends on external load and, specifically in this case, on self–weight only.

Actually, SRT can reduce the difference between $\mathbf{x}_\beta$ and $\tilde{\mathbf{x}}_\beta$ by means of relative rigid–body motions between the primary and the secondary mirror. In formula, the actual configuration can be described as:

$$\tilde{\mathbf{x}}_\beta = \mathbf{T}_\beta + \mathbf{R}_\beta \mathbf{x}_\beta + \Delta\mathbf{u}_\beta \,, \tag{5}$$

Please cite this document as: F. Buffa, A. Causin, A. Cazzani, S. Poppi, G. Sanna, M. Solci, F. Stochino, and E. Turco "The Sardinia Radio Telescope: A comparison between close-range photogrammetry and finite element models" Mathematics and Mechanics of Solids, 2017, Vol. 22(5): 1005-1026 doi:10.1177/1081286515616227

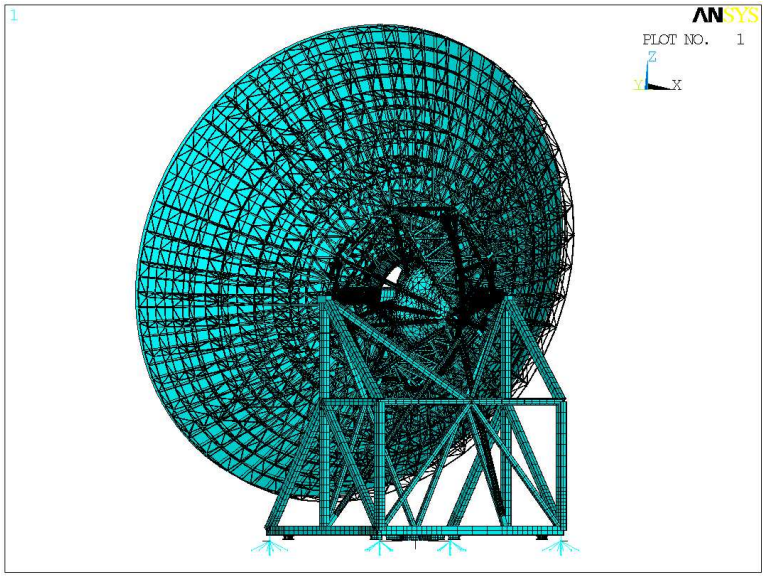

FIGURE 8. Back view of the SRT FE model (without the Thermal Shield) at elevation 15°.

where $\mathbf{T}_\beta$ and $\mathbf{R}_\beta$ represent, respectively, the translation matrix and the rotation matrix (associated to this rigid–body motion), while the increment of displacement $\Delta\mathbf{u}_\beta$ comes out by depurating $\mathbf{u}_\beta$ from the above mentioned rigid-body motion. The value of the parameters defining this rigid-body motion are determined by means of an Iterative Closest Point (ICP) algorithm, see [10, 11]. This algorithm can minimize the difference between two clouds of points. The reference point cloud is kept fixed, while the other one, the source, is transformed to best match the reference one. The transformation consists of a combination of a rigid rotation and translation of the source cloud. ICP iteratively revises the transformation in order to minimize the distance from the source to the reference point cloud. The a–th electro–mechanical actuator controls p mirror panels (where p can either be 2 or 4) by means of its elongation d_a. The procedure to compute the actuators elongation works like this:

(1) first the average normal vector $\mathbf{v}_a$ corresponding to the a–th actuator is evaluated:

$$\mathbf{v}_a = \left(\frac{1}{p} \sum_{i=1}^{p} \mathbf{n}_{a_i} \right), \tag{6}$$

where $\mathbf{n}_{a_i}$ is the unit vector along the normal to the i–th panel controlled by the a-th actuator.

(2) then, a unit vector $\hat{\mathbf{v}}_a$ is computed from $\mathbf{v}_a$; finally, the elongation d_a results as:

$$d_a = \hat{\mathbf{v}}_a \cdot \Delta\mathbf{u}_{\beta_a} . \tag{7}$$

In the following sections comparison between the FE model with (denoted by TS) and without thermal shield (denoted by NTS) and CRP data is provided in terms of such actuators elongations, evaluated point–wise and globally by means of Root Mean Square deviation,

Please cite this document as: F. Buffa, A. Causin, A. Cazzani, S. Poppi, G. Sanna, M. Solci, F. Stochino, and E. Turco "The Sardinia Radio Telescope: A comparison between close-range photogrammetry and finite element models" Mathematics and Mechanics of Solids, 2017, Vol. 22(5): 1005-1026 doi:10.1177/1081286515616227

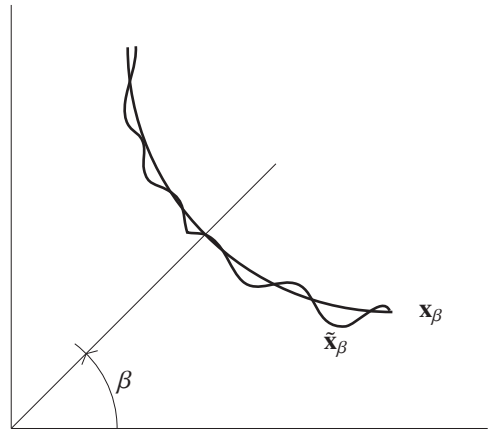

FIGURE 9. Sketch of the optimal $\mathbf{x}_\beta$ and of the actual $\tilde{\mathbf{x}}_\beta$ configuration of the SRT.

Δ_{RMS}, defined as:

$$\Delta_{RMS} = \sqrt{\frac{1}{n}\sum_{i=1}^{n}(\tilde{d}_i - d_i)^2}\,, \tag{8}$$

between two sets of n elongations $\tilde{d}_i$ and d_i. In the case of SRT the number n of actuators belonging to the principal mirror is 1104.

5.1. **Comparison between TS FE and NTS FE models.** In order to develop a thorough analysis of the structural influence of the thermal shield several comparisons between the model with and without thermal shield have been performed. For the sake of conciseness the configuration characterized by 90° elevation under gravitational loads has been considered only. In Figures 10–15 the displacements in the x–,y–, and z–direction are reported for the two FE models (TS and NTS). Very little differences can be seen considering the principal mirror displacements presented in Figures 10–12; these become negligible when considering a whole view like those presented in Figures 13–15. Furthermore if such global displacements are transformed into the required actuator displacements, which are necessary to correct the surface shape, (see Figures 16) the differences are still very little.

In order to highlight these differences the actuators displacements have been evaluated for other two elevation angles (15°, 60°) by means of the TS model (see Figure 7) and of the NTS model (see Figure 8).

The local difference are reported in the following Figures 17–19. The chromatic scale limits are different with respect to the other sections with the aim of highlighting the very small differences between the two models.

Figure 17 reports the situation belonging to 15° elevation where the thermal shield produces some interesting effect in the top central part of the principal mirror and on the outer circular ring. The maximum value of the local difference, defined as:

$$\Delta_{max} = \max_{i=1,\dots n} \mid \tilde{d}_i - d_i \mid, \tag{9}$$

is $\Delta_{max} < 0.5$ mm, while the corresponding global Δ_{RMS} is 0.212 mm.

Please cite this document as: F. Buffa, A. Causin, A. Cazzani, S. Poppi, G. Sanna, M. Solci, F. Stochino, and E. Turco "The Sardinia Radio Telescope: A comparison between close-range photogrammetry and finite element models" Mathematics and Mechanics of Solids, 2017, Vol. 22(5): 1005-1026 doi:10.1177/1081286515616227

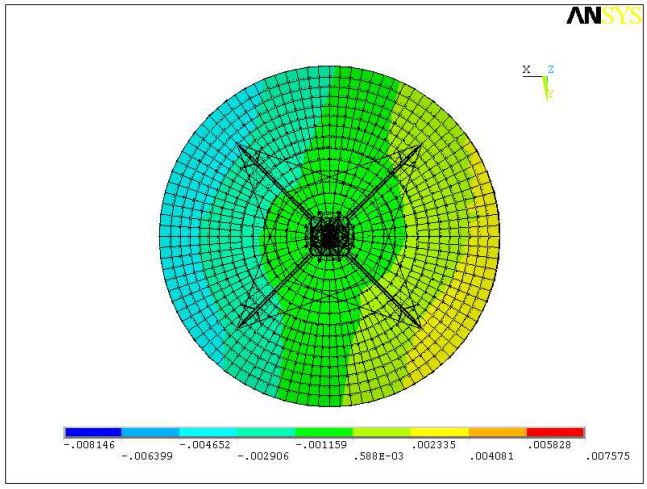

(a) TS model

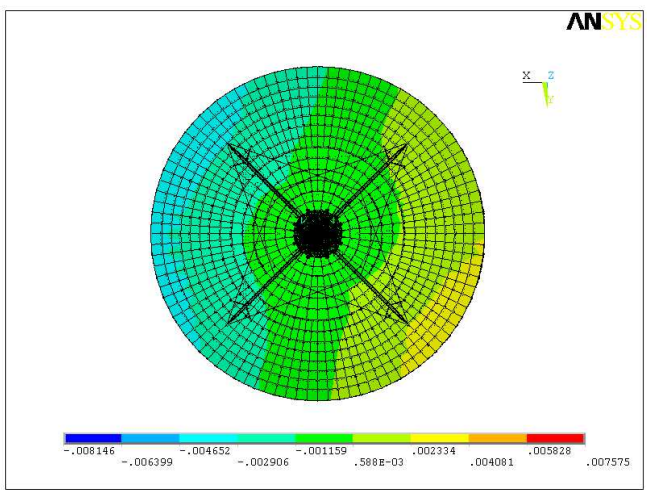

(b) NTS model

FIGURE 10. FE model displacements along the x–direction at 90° elevation: view of the principal mirror (the unit of the chromatic scale is m).

Figure 18 reports the 60° elevation case, where the thermal shield produces some interesting effect only on the top central part of the principal mirror. In this case, $\Delta_{max} < 0.3$ mm and $\Delta_{RMS} = 0.109$ mm.

Finally, Figure 19 reports the 90° elevation configuration corresponding to the principal mirror orthogonal to the vertical axis. In this case, the thermal shield produces non negligible effect on the whole principal mirror. In particular there is a characteristic symmetry

Please cite this document as: F. Buffa, A. Causin, A. Cazzani, S. Poppi, G. Sanna, M. Solci, F. Stochino, and E. Turco "The Sardinia Radio Telescope: A comparison between close-range photogrammetry and finite element models" Mathematics and Mechanics of Solids, 2017, Vol. 22(5): 1005-1026 doi:10.1177/1081286515616227

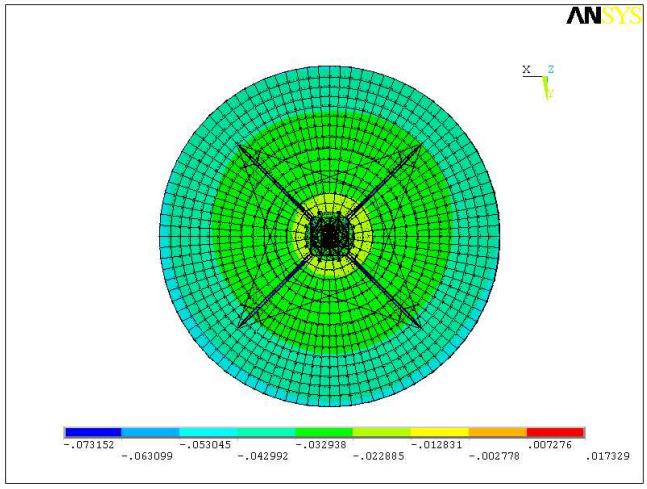

(a) TS model

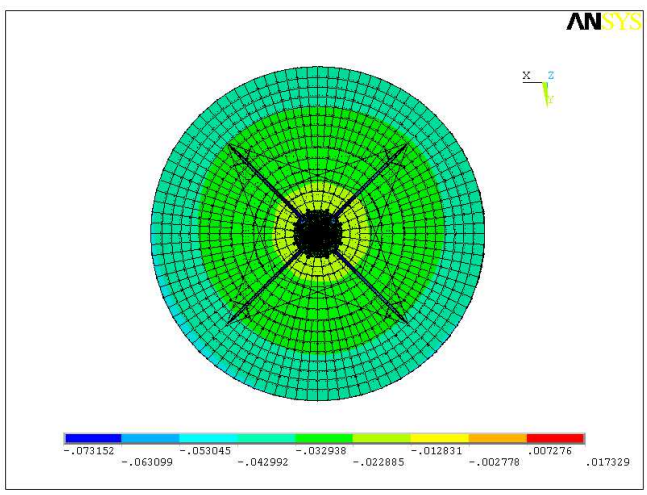

(b) NTS model

FIGURE 11. FE model displacements along the y-direction at 90° elevation: view of the principal mirror (the unit of the chromatic scale is m).

between the top–bottom and inner–outer circular ring parts. This time, $\Delta_{max} = 0.5$ mm, while the corresponding $\Delta_{RMS} = 0.271$ mm.

According to the aim of this paper (FE model analysis compared to field benchmark data provided by CRP) the most important comparison between the TS and NTS models is developed in Table 1, where the deviations of actuators displacements coming from FE analysis and CRP field recordings are presented. As it was expected the NTS model produces results more similar to CRP data than the those produced by the TS model. In

Please cite this document as: F. Buffa, A. Causin, A. Cazzani, S. Poppi, G. Sanna, M. Solci, F. Stochino, and E. Turco "The Sardinia Radio Telescope: A comparison between close-range photogrammetry and finite element models" Mathematics and Mechanics of Solids, 2017, Vol. 22(5): 1005-1026 doi:10.1177/1081286515616227

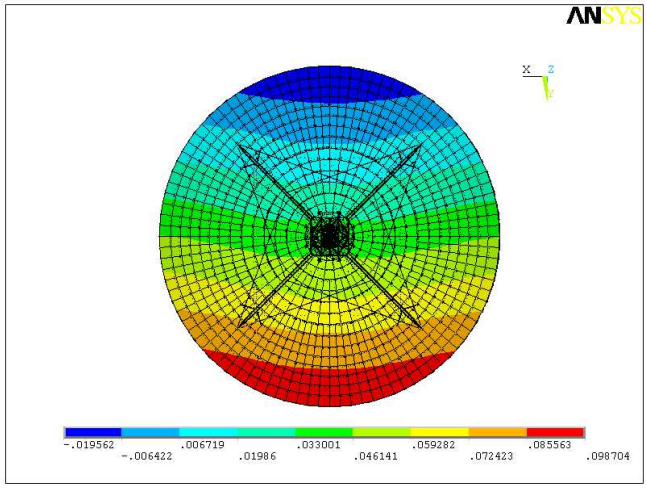

(a) TS model

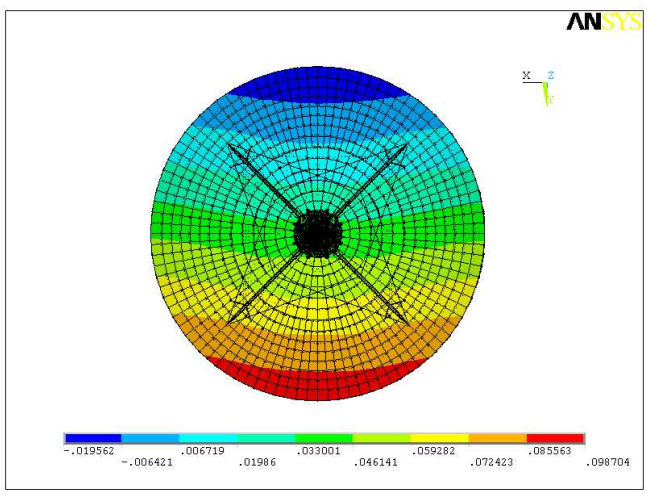

(b) NTS model

FIGURE 12. FE model displacements along the z-direction at 90° elevation: view of the principal mirror (the unit of the chromatic scale is m).

particular the former provides a minimum $\Delta_{RMS} = 0.491$ mm corresponding to an elevation angle of 60°, while the maximum is 0.814 mm for an elevation angle of 90°. In case of 15° Δ_{RMS} is 0.507 mm. The best improvement descending from assuming the NTS model instead of the TS one is obtained for the 15° elevation and corresponds to 12% . This confirms the influence on the mechanical behavior of the thermal shield which is not present in the real structure and not easily detectable by the direct absolute displacements comparisons.

Please cite this document as: F. Buffa, A. Causin, A. Cazzani, S. Poppi, G. Sanna, M. Solci, F. Stochino, and E. Turco "The Sardinia Radio Telescope: A comparison between close-range photogrammetry and finite element models" Mathematics and Mechanics of Solids, 2017, Vol. 22(5): 1005-1026 doi:10.1177/1081286515616227

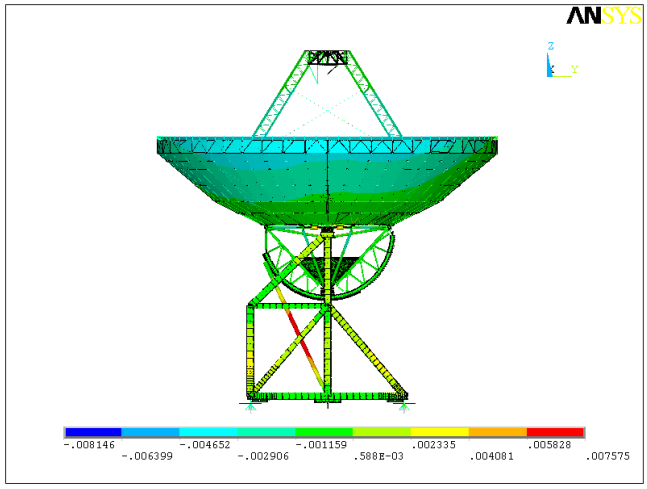

(a) TS model

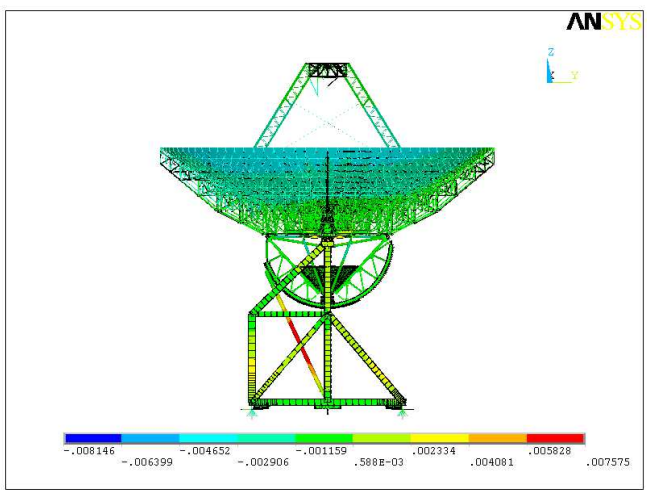

(b) NTS model

FIGURE 13. FE model displacements along the x–direction at 90° elevation: side view (the unit of the chromatic scale is m).

5.2. **Comparison between FE model without thermal shield and photogrammetric data.** As proven in the previous paragraph the FE model without the thermal shield provides the most realistic picture of the actual behavior of SRT. Local actuators displacements errors are presented in the sequel (see Figures 20–22). Actuators elongations have been estimated by means of the NTS FE model of SRT, see Figure 8 for different configurations. Figures 20–22, referring to the configurations corresponding to three different elevation angles (15°, 60°, 90°) depicts the local differences between the actuators displacements

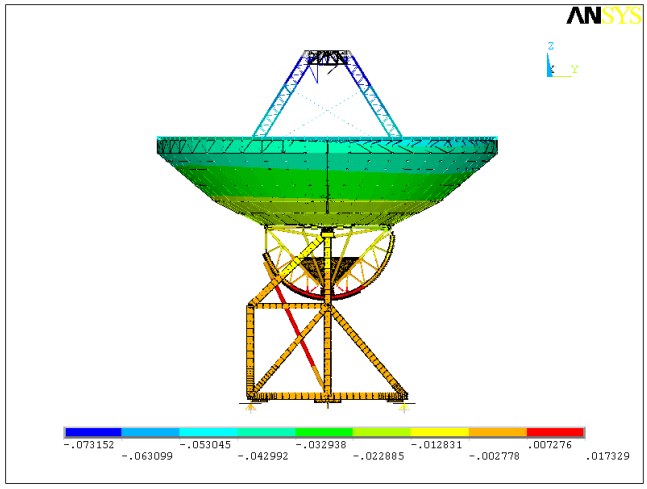

(a) TS model

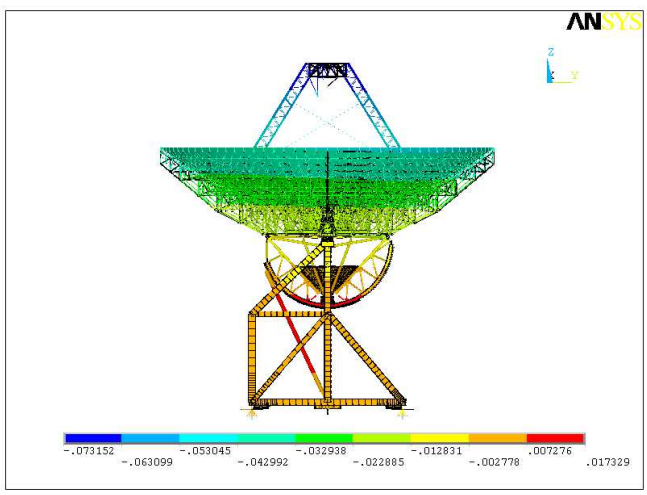

(b) NTS model

FIGURE 14. FE model displacements along the y–direction at 90° elevation: side view (the unit of the chromatic scale is m).

produced by the numerical model and CRP data. The larger differences can be observed at 90° elevation ($\Delta_{RMS} = 0.814$ mm, with local differences very high in the bottom part of the mirror); while the lowest ones are seen in the 60° elevation ($\Delta_{RMS} = 0.491$ mm, with a rather uniform distribution of the local differences). Probably the weight distribution when the principal mirror lies parallel to the horizon (90°) produces a structural response which is described in a not enough accurate way by the model.

Please cite this document as: F. Buffa, A. Causin, A. Cazzani, S. Poppi, G. Sanna, M. Solci, F. Stochino, and E. Turco "The Sardinia Radio Telescope: A comparison between close-range photogrammetry and finite element models" Mathematics and Mechanics of Solids, 2017, Vol. 22(5): 1005-1026 doi:10.1177/1081286515616227

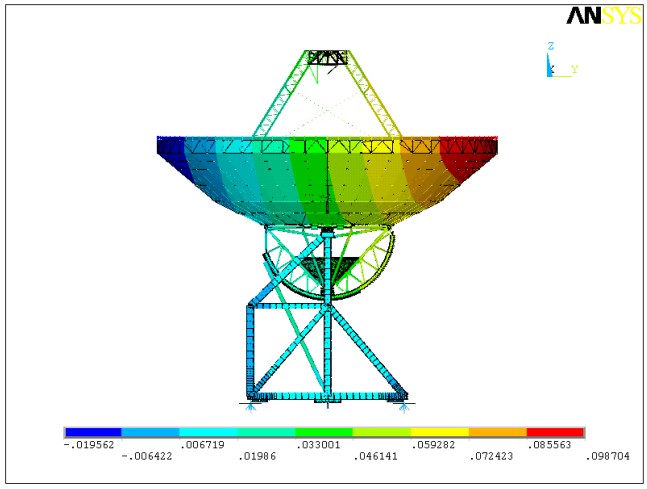

(a) TS model

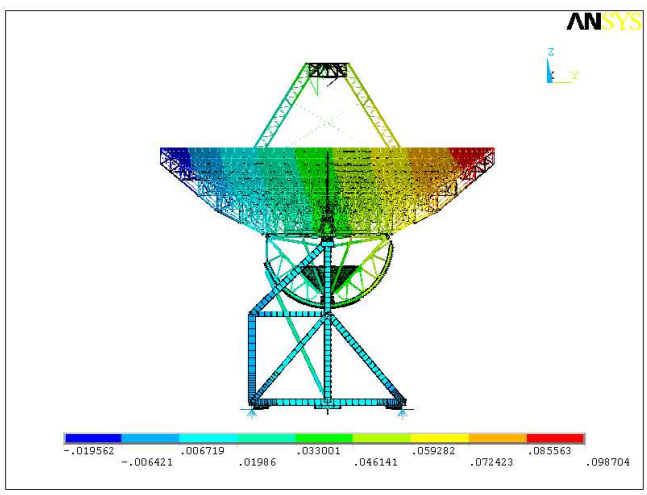

(b) NTS model

FIGURE 15. FE model displacements along the z–direction at 90° elevation: side view (the unit of the chromatic scale is m).

6. Conclusions and new research perspectives

Numerical simulations make evident that the FE model has to be updated in order to adequately match the photogrammetric measurements. These can be considered as a kind of experimental test on the actual SRT structure. Among the extended bibliography on model updating we recall the contributions, and references contained therein, of [12, 13, 14, 15] since they give the main guidelines on updating methodology and [16, 17, 18, 19, 20, 21, 22, 23, 24] as technical applications of updating.

Please cite this document as: F. Buffa, A. Causin, A. Cazzani, S. Poppi, G. Sanna, M. Solci, F. Stochino, and E. Turco "The Sardinia Radio Telescope: A comparison between close-range photogrammetry and finite element models" Mathematics and Mechanics of Solids, 2017, Vol. 22(5): 1005-1026 doi:10.1177/1081286515616227

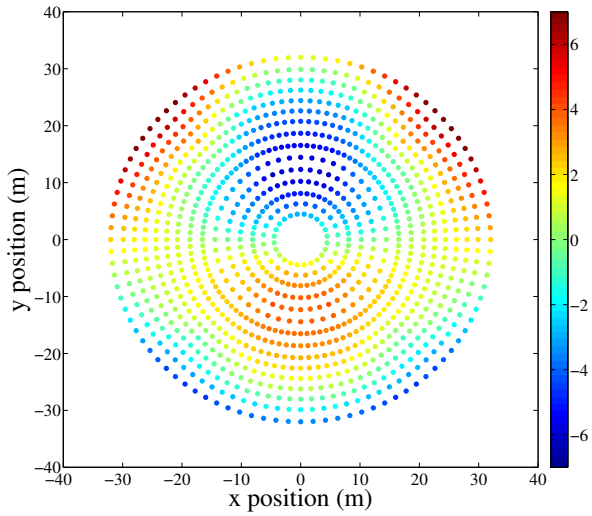

(a) TS model

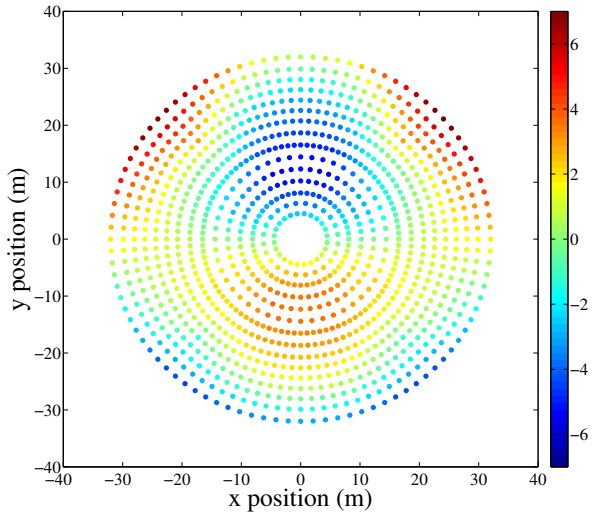

(b) NTS model

FIGURE 16. Actuators displacements estimated by means of FE models for 90° elevation (the unit of the chromatic scale is m).

In [25] there is a complete strategy to update the SRT finite element model. Here we sketch only the main guidelines and main papers which can profitably consulted. Updating strategies try to reduce differences between predicted data, by the finite element model, and measured data, in this case by photogrammetric measurements, by a suitable procedure which has to contain an effective filter for data errors. We follow the way used in [26, 27, 28, 29] which is based on the so–called Tikhonov's approach, see [30], and uses

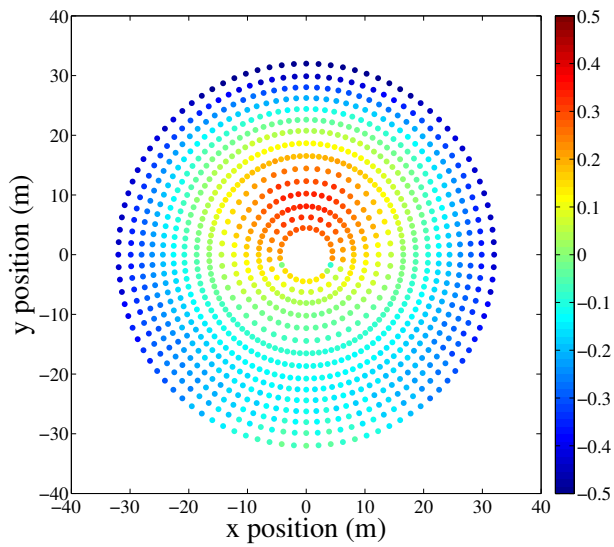

FIGURE 17. Difference of actuators displacements predicted by the TS and NTS FE models at 15° elevation, $\Delta_{RMS} = 0.212$ mm (chromatic scale of displacements is in mm).

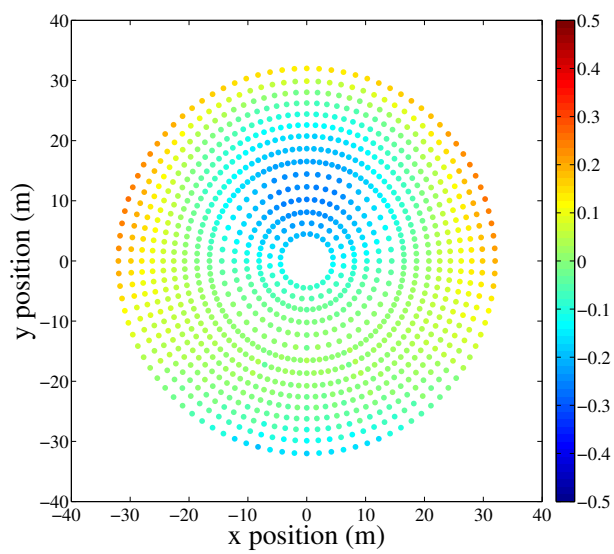

FIGURE 18. Difference of actuators displacements predicted by the TS and NTS FE models at 60° elevation, $\Delta_{RMS} = 0.109$ mm (chromatic scale of displacements is in mm).

Please cite this document as: F. Buffa, A. Causin, A. Cazzani, S. Poppi, G. Sanna, M. Solci, F. Stochino, and E. Turco "The Sardinia Radio Telescope: A comparison between close-range photogrammetry and finite element models" Mathematics and Mechanics of Solids, 2017, Vol. 22(5): 1005-1026 doi:10.1177/1081286515616227

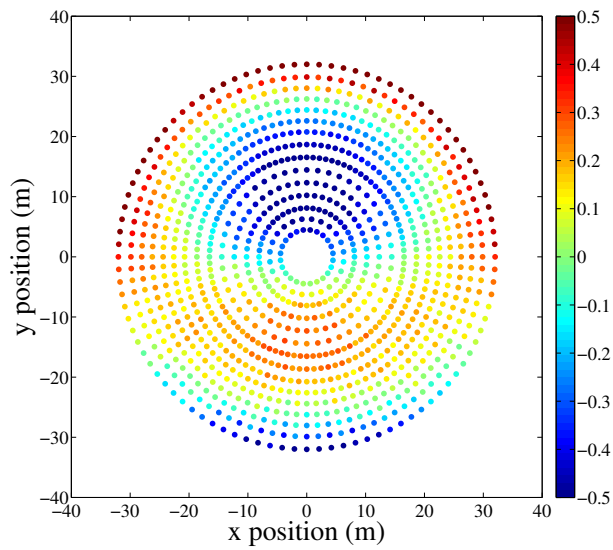

FIGURE 19. Difference of actuators displacements predicted by the TS and NTS FE models at 90° elevation, $\Delta_{RMS} = 0.271$ mm (chromatic scale of displacements is in mm).

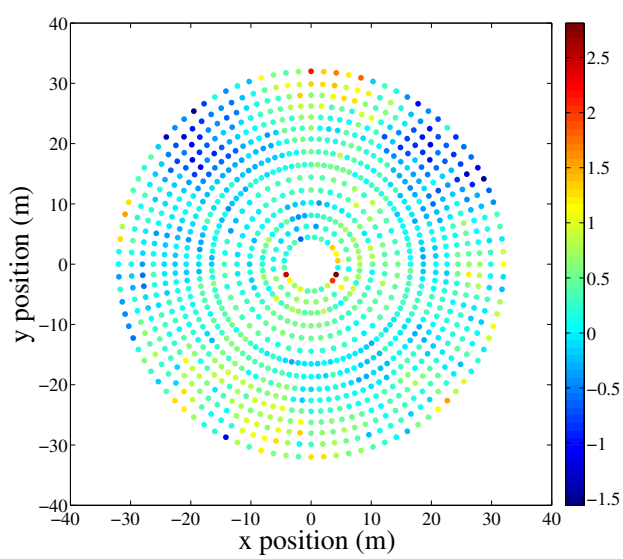

FIGURE 20. Difference of actuators displacements predicted by the NTS FE model and CRP at 15° elevation, $\Delta_{RMS} = 0.507$ mm (chromatic scale of displacements is in mm).

Please cite this document as: F. Buffa, A. Causin, A. Cazzani, S. Poppi, G. Sanna, M. Solci, F. Stochino, and E. Turco "The Sardinia Radio Telescope: A comparison between close-range photogrammetry and finite element models" Mathematics and Mechanics of Solids, 2017, Vol. 22(5): 1005-1026 doi:10.1177/1081286515616227

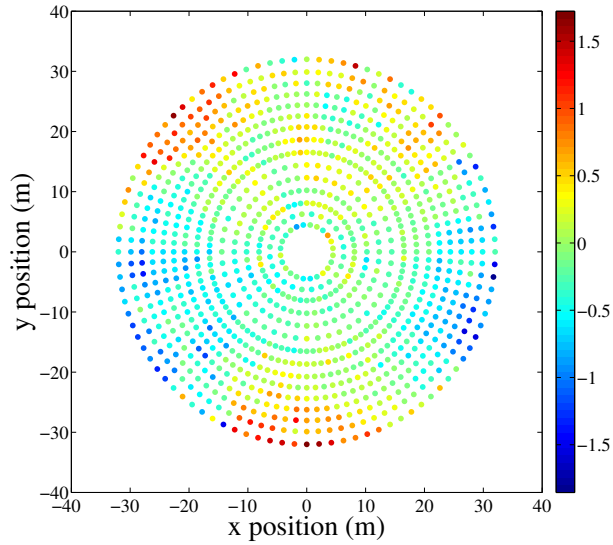

FIGURE 21. Difference of actuators displacements predicted by the NTS FE model and CRP at 60° elevation, $\Delta_{RMS} = 0.491$ mm (chromatic scale of displacements is in mm).

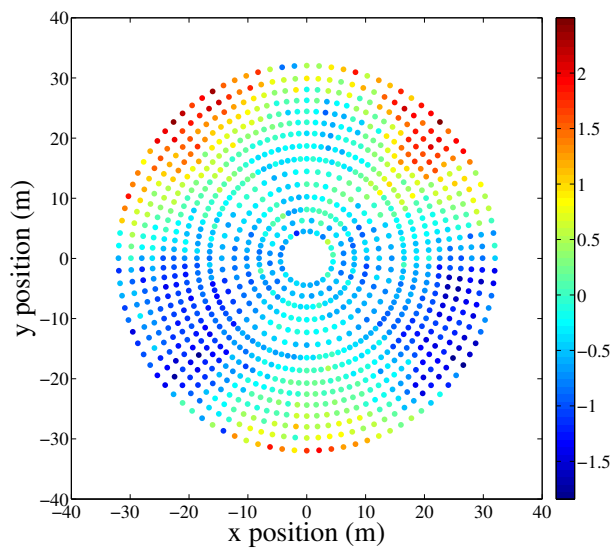

FIGURE 22. Difference of actuators displacements predicted by the NTS FE model and CRP at 90° elevation, $\Delta_{RMS} = 0.814$ mm (chromatic scale of displacements is in mm).

Please cite this document as: F. Buffa, A. Causin, A. Cazzani, S. Poppi, G. Sanna, M. Solci, F. Stochino, and E. Turco "The Sardinia Radio Telescope: A comparison between close-range photogrammetry and finite element models" Mathematics and Mechanics of Solids, 2017, Vol. 22(5): 1005-1026 doi:10.1177/1081286515616227

TABLE 1. Global Root Mean Square Error of FE models compared to the CRP.

Elevation β	Δ_{RMS} (mm)		% improvement
	TS	NTS	
15°	0.5751	0.5068	12%
60°	0.5239	0.4907	6%
90°	0.8441	0.8138	4%

numerical tools such as Singular Value Decomposition, [31], [32] and [33], and the Generalized Cross–Validation criterion to filter the data errors, proposed in [34] and extensively tested in [35, 36].

Finally, we remark that the results of this research line could also be useful to enrich refined numerical model such as those reported in [37, 38] for beams, those based on mixed and hybrid finite elements, see [39, 40, 41], which provide more accurate stress description also in the case of layered structures [42] and those based on the so–called isogeometric approach [37, 38, 43, 44].

In addition, the authors report below a series of fields where an improved numerical model can be profitably used:

- *Buckling problems* as those described in [45, 46, 47, 48] and the papers cited therein. These problems are very sensitive to the stress level achieved and therefore could benefit from its accurate description.
- *New materials* require refined mathematical models to describe them; some authors use suitable parameters, see [49, 50, 51, 52], paying particular attention to cases which leads to non–unique and non–stable solutions, see [53, 54, 55]; alternatively, there is the way followed in [56, 57] where a concentrated damage model for an interfacial zone is developed; in addition, the application of higher continuum models can be attractive, see for example [58, 59, 60, 61].
- *Damage detection* is a an emerging and important field which deserves particular attention, see for example the works [62, 63] which consider traveling loads as signal or in identification problems such as those described in [64, 65, 66, 67, 68, 69].
- *Plasticity problems* regarding the evaluation of the collapse load, see [70, 71, 72, 73, 74, 75] and the variational techniques presented in [76] for dissipative phenomena.
- *Smart and piezoelectric materials* might be advantageously used for an effective structural control, see *e.g.* [77, 78].

ACKNOWLEDGEMENT

The financial support of RAS, the Autonomous Region of Sardinia, under grant number CRP-26658 (L. R. 7/2007, year 2011 call, Project: *Deformation estimates of the Sardinia Radio Telescope*) is gratefully acknowledged.

REFERENCES

[1] J. W. M. Baars. *The Paraboloidal Reflector Antenna in Radio Astronomy and Communication*, volume 348 of *Astrophysics and Space Science Library*. Springer, 2007.

[2] J. Ruze. Antenna tolerance theory – a review. *Proc. IEEE*, 54:633–640, 1966.

Please cite this document as: F. Buffa, A. Causin, A. Cazzani, S. Poppi, G. Sanna, M. Solci, F. Stochino, and E. Turco "The Sardinia Radio Telescope: A comparison between close-range photogrammetry and finite element models" Mathematics and Mechanics of Solids, 2017, Vol. 22(5): 1005-1026 doi:10.1177/1081286515616227

[3] J. W. Findlay. Antennas and receivers for radio astronomy. *Advances in Radio Research*, 2:37–119, 1964.
[4] M. Süss, D. Koch, and H. Paluszek. The Sardinia Radio Telescope (SRT) optical alignment. In *Ground–based and Airborne Telescopes IV. Proceedings of SPIEE*, number 84442G, pages 1–16, doi:10.1117/12.926141, 2012.
[5] N. D'Amico. Private communication. 2012.
[6] G. Zacchiroli, F. Fiocchi, G. Maccaferri, M. Morsiani, C. Pernechele, T. Pisanu, J. Roda, and G. Vargiu. The panels for primary and secondary mirror reflectors and the active surface system for the new Sardinia Radio Telescope. *Memorie della Società Astronomica Italiana Supplement*, 10:126, 2006.
[7] T. Luhmann, S. Robson, S. Kyle, and I. Harley. *Close Range Photogrammetry Principles, techniques and applications*. Whittles Publishing, 2006.
[8] O. C. Zienkiewicz. *The finite element method*. McGraw–Hill, London, 3rd edition edition, 1977.
[9] ANSYS Inc. *ANSYS, Inc. Release notes*. Canonsburg, PA, 2009.
[10] P. J. Besl and N. D. McKay. A method for registration of 3–D shapes. *IEEE Trans. on Pattern Analysis and Machine Intelligence*, 14(2):239–256, 1992.
[11] J. C. Simo and R. L. Taylor. Consistent tangent operators for rate–independent elastoplasticity. *Computer Methods in Applied Mechanics and Engineering*, 48(1):101–118, 1985.
[12] M. I. Friswell and J. E. Mottershead. *Finite element model updating in structural dynamics*. Kluwer Academic Publisher, 1995.
[13] A. Aktan, N. Catbas, N. Türer, and Z. Zhang. Structural identification: analytical aspects. *Journal of Structural Engineering*, 124(7):817–829, 1998.
[14] A. De Sortis, E. Antonacci, and F. Vestroni. Dynamic identification of a masonry building using forced vibration tests. *Engineering Structures*, 27(2):155–165, 2005.
[15] Y. Wang and T. Zhang. Finite element model updating using estimation of distribution algorithms. In *Sixty International Conference on Structural Health Monitoring of Intelligent Infrastructure*, 2013.
[16] M. Dilena and A. Morassi. Dynamic testing of damaged bridge. *Mechanical Systems and Signal Processing*, 25:1485–1507, 2011.
[17] M. Dilena, A. Morassi, and M. Perin. Dynamic identification of a reinforced concrete damaged bridge. *Mechanical Systems and Signal Processing*, 25:2990–3009, 2011.
[18] A. Morassi. Dynamic testing and structural identification of the Hypo Bank office complex. I: Experiments. *Journal of Structural Engineering ASCE*, 137(12):1527–1539, 2011.
[19] A. Morassi and F. Polentarutti. Dynamic testing and structural identification of the Hypo Bank office complex. II: Identification. *Journal of Structural Engineering ASCE*, 137(12):1540–1552, 2011.
[20] S. Bennati, L. Nardini, and W. Salvatore. Dynamic behavior of a medieval masonry bell tower. part I: Experimental measurements and modeling of bell's dynamic actions. *Journal of Structural Engineering*, 131(11):1647–1655, 2005.
[21] B. Moaveni and I. Behmanesh. Effects of changing ambient temperature on finite element model updating of the Dowling Hall Footbridge. *Engineering Structures*, 43:58–68, 2012.
[22] B. Richard, L. Adelaide, C. Cremona, and A. Orcesi. A methodology for robust updating of nonlinear structural models. *Engineering Structures*, 41(356–372), 2012.

Please cite this document as: F. Buffa, A. Causin, A. Cazzani, S. Poppi, G. Sanna, M. Solci, F. Stochino, and E. Turco "The Sardinia Radio Telescope: A comparison between close-range photogrammetry and finite element models" Mathematics and Mechanics of Solids, 2017, Vol. 22(5): 1005-1026 doi:10.1177/1081286515616227

[23] B. A. Zárate and J. M. Caicedo. Finite element model updating: Multiple alternatives. *Engineering Structures*, 30:3724–3730, 2008.

[24] H. Schlune, M. Plos, and K. Gylltoft. Improved bridge evaluation through finite element model updating using static and dynamic measurements. *Engineering Structures*, 31:1477–1485, 2009.

[25] F. Stochino, A. Cazzani, S. Poppi, and E. Turco. Sardinia Radio Telescope finite element model updating by means of photogrammetric measurements. *Mathematics and Mechanics of Solids*, accepted for publication, 2014.

[26] E. Turco. Load distribution modelling for pin-jointed trusses by an inverse approach. *Computer Methods in Applied Mechanics and Engineering*, 165:291–306, 1998.

[27] E. Turco. A boundary elements approach to identify static boundary conditions in elastic solids from stresses at internal points. *Inverse Problems in Engineering*, 7:309–333, 1999.

[28] E. Turco. Is the statistical approach suitable for identyfing actions on structures? *Computers and Structures*, 83:2112–2120, 2005.

[29] E. Turco. Identification of axial forces on statically indeterminate pin–jointed trusses by a nondestructive mechanical test. *The Open Civil Engineering Journal*, 7:50–57, 2013.

[30] A. N. Tikhonov and V. Y. Arsenin. *Solution of ill–posed problems*. John Wiley & Sons, New York, 1977.

[31] G. H. Golub and C. F. Van Loan. *Matrix computations*. The Johns Hopkins University Press, Baltimore and London, 3rd edition, 1996.

[32] P. C. Hansen. Numerical tools for analysis and solution of Fredholm integral equations of the first kind. *Inverse Problems*, 8:849–872, 1992.

[33] S. Pellegrino. Structural computations with the singular value decomposition of the equilibrium matrix. *International Journal of Solids and Structures*, 30(21):3025–3035, 1993.

[34] G. H. Golub, M. Health, and G. Wahba. Generalized Cross–Validation as a method for choosing a good ridge parameter. *Technometrics*, 21(2):215–223, May 1979.

[35] A. Bilotta and E. Turco. A numerical study on the solution of the Cauchy problem in elasticity. *International Journal of Solids and Structures*, 46:4451–4477, 2009.

[36] E. Turco. An effective algorithm for reconstructing boundary conditions in elastic solids. *Computer Methods in Applied Mechanics and Engineering*, 190:3819–3829, 2001.

[37] A. Cazzani, M. Malagù, and E. Turco. Isogeometric analysis of plane curved beams. *Mathematics and Mechanics of Solids*, published online 20 April 2014, DOI: 10.1177/1081286514531265:1–16, 2014.

[38] A. Cazzani, M. Malagù, F. Stochino, and E. Turco. Constitutive models for strongly curved beams in the frame of isogeometric analysis. *Mathematics and Mechanics of Solids*, (in print), 2014.

[39] S. N. Atluri and A. Cazzani. Rotations in computational solid mechanics. *Archives of Computational Methods in Engineering*, 2:49–138, 1995.

[40] A. Cazzani and S. N. Atluri. Four–noded mixed finite elements, using unsymmetric stresses, for linear analysis of membranes. *Computational Mechanics*, 11:229–251, 1993.

[41] A. Cazzani and C. Lovadina. On some mixed finite element methods for plane membrane problems. *Computational Mechanics*, 20:560–572, 1997.

Please cite this document as: F. Buffa, A. Causin, A. Cazzani, S. Poppi, G. Sanna, M. Solci, F. Stochino, and E. Turco "The Sardinia Radio Telescope: A comparison between close-range photogrammetry and finite element models" Mathematics and Mechanics of Solids, 2017, Vol. 22(5): 1005-1026 doi:10.1177/1081286515616227

[42] A. Cazzani, E. Garusi, A. Tralli, and S. N. Atluri. A four–node hybrid assumed-strain finite element for laminated composite plates. *Computers, Materials & Continua*, 2:23–38, 2005.

[43] Antonio Cazzani, Marcello Malagù, and Emilio Turco. Isogeometric analysis: a powerful numerical tool for the elastic analysis of historical masonry arches. *Continuum Mechanics and Thermodynamics*, published online 28 December 2014, DOI: 10.1007/s00161-014-0409-y:1–18, 2014.

[44] A. Bilotta, G. Formica, and E. Turco. Performance of a high–continuity finite element in three–dimensional elasticity. *International Journal for Numerical Methods in Biomedical Engineering (Communications in Numerical Methods in Engineering)*, 26:1155–1175, 2010.

[45] M. Pignataro and A. Luongo. Asymmetric interactive buckling of thin–walled columns with initial imperfections. *Thin–Walled Structures*, 5(5):365–382, 1987.

[46] A Luongo. Mode localization in dynamics and buckling of linear imperfect continuous structures. *Nonlinear Dynamics*, 25(1-3):133–156, 2001.

[47] A. Luongo. On the amplitude modulation and localization phenomena in interactive buckling problems. *International Journal of Solids and Structures*, 27(15):1943–1954, 1991.

[48] M. Pignataro, A. Luongo, and N. Rizzi. On the effect of the local overall interaction on the postbuckling of uniformly compressed channels. *Thin–Walled Structures*, 3(4):293–321, 1985.

[49] A. Rinaldi and L. Placidi. A microscale second gradient approximation of the damage parameter of quasi–brittle heterogeneous lattices. *ZAMM - Zeitschrift für Angewandte Mathematik und Mechanik*, 1(16):DOI 10.1002/zamm.201300028, 2013.

[50] A. Rinaldi. A rational model for 2D disordered lattices under uniaxial loading. *International Journal of Damage Mechanics*, 18:233–257, 2009.

[51] A. Rinaldi. Statistical model with two order parameters for ductile and statistical model with two order parameters for ductile and soft fiber bundles in nanoscience and biomaterials. *Physical Review E (Statistical, Nonlinear, and Soft Matter Physics)*, 83(046126(10)), 2011.

[52] A. Madeo, L. Placidi, and G. Rosi. Towards the design of metamaterials with enhanced damage sensitivity: second gradient porous materials. *Research in Nondestructive Evaluation*, 25(2):99–124, 2014.

[53] V. A. Eremeyev and W. Pietraszkiewicz. The nonlinear theory of elastic shells with phase transitions. *Journal of Elasticity*, 74(1):67–86, 2004.

[54] V. A. Yeremeyev, A. B. Freidin, and L. L. Sharipova. The stability of the equilibrium of two-phase elastic solids. *Journal of Applied Mathematics and Mechanics*, 71(1):61–84, 2007.

[55] V. A. Eremeev, A. B. Freidin, and L. L. Sharipova. Nonuniqueness and stability in problems of equilibrium of elastic two–phase bodies. *Doklady Physics*, 48(7):359–363, 2003.

[56] F. dell'Isola and A. Romano. On the derivation of thermomechanical balance equations for continuous systems with a nonmaterial interface. *International Journal of Engineering Science*, 25(11-12):1459–1468, 1987.

[57] F. D'Annibale and A. Luongo. A damage constitutive model for sliding friction coupled to wear. *Continuum Mechanics and Thermodynamics*, 25(2-4):503–522, 2013.

[58] F. dell'Isola, P. Seppecher, and A. Madeo. How contact interactions may depend on the shape of cauchy cuts in n-th gradient continua: approach á la D'Alembert.

Please cite this document as: F. Buffa, A. Causin, A. Cazzani, S. Poppi, G. Sanna, M. Solci, F. Stochino, and E. Turco "The Sardinia Radio Telescope: A comparison between close-range photogrammetry and finite element models" Mathematics and Mechanics of Solids, 2017, Vol. 22(5): 1005-1026 doi:10.1177/1081286515616227

Zeitschrift für Angewandte Mathematik und Physik (ZAMP), 63(6):1119–1141, 2012.

[59] F. dell'Isola and P. Seppecher. The relationship between edge contact forces, double forces and interstitial working allowed by the principle of virtual power. *Comptes Rendus de l'Academie de Sciences - Serie IIb: Mecanique, Physique, Chimie, Astronomie*, 321:303–308, 1995.

[60] S. Federico, A. Grillo, S. Imatani, G. Giaquinta, and W. Herzog. An energetic approach to the analysis of anisotropic hyperelastic materials. *International Journal of Engineering Science*, 46:164–181, 2008.

[61] A. Misra. Mechanistic model for contact between rough surfaces. *Journal of Engineering mechanics*, 123(5):475–484, 1997.

[62] N. Roveri and A. Carcaterra. Damage detection in structures under travelling loads by the Hilbert–Huang transform. *Mechanical System and Signal Processing*, 28:128–144, 2012.

[63] M. Ferretti and G. Piccardo. Dynamic modeling of taut strings carrying a traveling mass. *Continuum Mechanics and Thermodynamics*, 25(2-4):469–488, 2013.

[64] E. Turco. A strategy to identify exciting forces acting on structures. *International Journal for Numerical Methods in Engineering*, 64:1483–1508, 2005.

[65] G. Alessandrini, A. Bilotta, G. Formica, A. Morassi, E. Rosset, and E. Turco. Evaluating the volume of a hidden inclusion in an elastic body. *Journal of Computational and Applied Mathematics*, 198(2):288–306, 2007.

[66] G. Alessandrini, A. Bilotta, G. Formica, A. Morassi, E. Rosset, and E. Turco. Numerical size estimates of inclusions in elastic bodies. *Inverse Problems*, 21:133–151, 2005.

[67] G. Alessandrini, A. Bilotta, A. Morassi, and E. Turco. Computing volume bounds of inclusions by EIT measurements. *Journal of Scientific Computing*, 33(3):293–312, 2007.

[68] Y. Wang and H. Hao. Damage identification scheme based on compressive sensing. *Journal of Computing in Civil Engineering (ASCE)*, 04014037:1–10, 2014.

[69] A. Bilotta and E. Turco. Numerical sensitivity analysis of corrosion detection. *Mathematics and Mechanics of Solids*, DOI: 10.1177/1081286514560093:1–17, 2014.

[70] R. Contro, C. Poggi, and A. Cazzani. Numerical analysis of fire effects on beam structures. *Engineering Computations*, 5:53–58, 1988.

[71] A. Cazzani, R. Contro, and L. Corradi. On the evaluation of the shakedown boundary for temperature-dependent elastic properties. *European Journal of Mechanics A/Solids*, 11:539–550, 1992.

[72] U. Andreaus and P. Baragatti. Cracked beam identification by numerically analysing the nonlinear behaviour of the harmonically forced response. *Journal of Sound and Vibration*, 330(4):721–742, 2011.

[73] A. Cazzani and M. Rovati. Sensitivity analysis and optimum design of elastic-plastic structural systems. *Meccanica*, 26:173–178, 1991.

[74] E. Turco and P. Caracciolo. Elasto–plastic analysis of Kirchhoff plates by high simplicity finite elements. *Computer Methods in Applied Mechanics and Engineering*, 190:691–706, 2000.

[75] P. Neff, A. Sysow, and C. Wieners. Numerical approximation of incremental infinitesimal gradient plasticity. *International Journal for Numerical Methods in Engineering*, 77:414–436, 2009.

[76] F. dell'Isola, A. Madeo, and P. Seppecher. Boundary conditions at fluid–permeable interfaces in porous media: A variational approach. *International Journal of Solids*

Please cite this document as: F. Buffa, A. Causin, A. Cazzani, S. Poppi, G. Sanna, M. Solci, F. Stochino, and E. Turco "The Sardinia Radio Telescope: A comparison between close-range photogrammetry and finite element models" Mathematics and Mechanics of Solids, 2017, Vol. 22(5): 1005-1026 doi:10.1177/1081286515616227

and Structures, 46(17):3150–3164, 2009.

[77] C. Maurini, J. Pouget, and F. dell'Isola. Extension of the Euler–Bernoulli model of piezoelectric laminates to include 3D effects via a mixed approach. *Computers and Structures*, 84:1438–1458, 2006.

[78] R. C. Batra, F. dell'Isola, S. Vidoli, and D. Vigilante. Multimode vibration suppression with passive two-terminal distributed network incorporating piezoceramic transducers. *International Journal of Solids and Structures*, 42:3115–3132, 2005.

INAF–OAC Osservatorio Astronomico di Cagliari, via della Scienza 5, 09047 Selargius (CA) Italia.
Email address: fbuffa@oa-cagliari.inaf.it

DADU, Università degli Studi di Sassari, Asilo Sella, via Garibaldi 35 07041 Alghero (SS), Italia.
Email address: acausin@uniss.it

DICAAR, Università degli Studi di Cagliari, via Marengo 2, 09123 Cagliari (CA) Italia.
Email address: antonio.cazzani@unica.it

INAF–OAC Osservatorio Astronomico di Cagliari, via della Scienza 5, 09047 Selargius (CA) Italia.
Email address: spoppi@oa-cagliari.inaf.it

DICAAR, Università degli Studi di Cagliari, via Marengo 2, 09123 Cagliari (CA) Italia
Email address: topoca@unica.it

DADU, Università degli Studi di Sassari, Asilo Sella, via Garibaldi 35 07041 Alghero (SS), Italia.
Email address: margherita@uniss.it

DADU, Università degli Studi di Sassari, Asilo Sella, via Garibaldi 35, 07041 Alghero (SS), Italia.
Email address: fstochino@uniss.it

DADU, Università degli Studi di Sassari, Asilo Sella, via Garibaldi 35 07041 Alghero (SS), Italia.
Email address, Corresponding author: emilio.turco@uniss.it

Please cite this document as: F. Buffa, A. Causin, A. Cazzani, S. Poppi, G. Sanna, M. Solci, F. Stochino, and E. Turco "The Sardinia Radio Telescope: A comparison between close-range photogrammetry and finite element models" Mathematics and Mechanics of Solids, 2017, Vol. 22(5): 1005-1026 doi:10.1177/1081286515616227